Structure-Reactivity Relationships in Multi-Component Transition Metal Oxide Catalysts
FINAL Report

DOE Award Number: DE-FG02-98ER14882
Applicant/Institution: Yale University
Street Address/City/State/Zip: P.O. Box 208337, New Haven, CT 06520-8337
Principal Investigator: Prof. Eric I. Altman
Address: Department of Chemical and Environmental Engineering
Yale University
PO Box 208260
New Haven, CT 06520-8260
Telephone Number: 203-432-4375
Email: eric.altman@yale.edu
DOE/Office of Science Program Office: Basic Energy Sciences
DOE/Office of Science Program Office Technical Contact: Dr. Raul Miranda
Period Covered: July 1998 – July 2015

Abstract

The focus of the project was on developing an atomic-level understanding of how transition metal oxide catalysts function. Over the course of several renewals the specific emphases shifted from understanding how local structure and oxidation state affect how molecules adsorb and react on the surfaces of binary oxide crystals to more complex systems where interactions between different transition metal oxide cations in an oxide catalyst can affect reactivity, and finally to the impact of cluster size on oxide stability and reactivity. Hallmarks of the work were the use of epitaxial growth methods to create surfaces relevant to catalysis yet tractable for fundamental surface science approaches, and the use of scanning tunneling microscopy to follow structural changes induced by reactions and to pinpoint adsorption sites. Key early findings included the identification of oxidation and reduction mechanisms on a tungsten oxide catalyst surface that determine the sites available for reaction, identification of C-O bond cleavage as the rate limiting step in alcohol dehydration reactions on the tungsten oxide surface, and demonstration that reduction does not change the favored reaction pathway but rather eases C-O bond cleavage and thus reduces the reaction barrier. Subsequently, a new reconstruction on the anatase phase of TiO_2 relevant to catalysis was discovered and shown to create sites with distinct reactivity compared to other TiO_2 surfaces. Building on this work on anatase, the mechanism by which TiO_2 enhances the reactivity of vanadium oxide layers was characterized and it was found that the TiO_2 substrate can force thin vanadia layers to adopt structures they would not ordinarily form in the bulk which in turn creates differences in reactivity between supported layers and bulk samples. From there, the work progressed to studying well-defined ternary oxides where synergistic effects between the two cations can induce catalytic properties not seen for the individual binary oxides and to the structure and properties of transition metal oxide clusters. For the latter, surprising results were found including the observation that small clusters can actually be orders of magnitude more difficult than bulk materials to oxidize and that even weak substrate interactions can

dictate the structure and reactivity of the oxide clusters. It was shown that these results could be explained in terms of simple thermodynamic arguments that extend to materials beyond the Co oxide system studied.

Report

1. Introduction

Transition metal oxides are widely used as heterogeneous catalysts in the chemical and energy industries. As partial oxidation catalysts, oxides are used to convert hydrocarbon feedstocks into more valuable alcohols, aldehydes, ketones, and acids. Improvements in activity and selectivity offer the promise of using less expensive feedstocks more efficiently, thus reducing waste generation and making better use of scarce resources. Oxides are also used to selectively reduce NO emitted from power plants and diesel vehicles where more active and selective catalysts can potentially reduce power generation costs while simultaneously reducing pollution.

The oxides of the early transition metals V, Mo, and W are active catalysts for a number of reactions including the partial oxidation of methanol to formaldehyde,[1,2] alkane metathesis,[3] and the selective catalytic reduction (SCR) of NO by NH_3.[4] The catalytic activity and function (i.e., oxidative dehydrogenation versus dehydration of alkoxide intermediates) of these materials is generally structure sensitive.[1,5-8] Because of the difficulty in preparing extended single crystals of the catalytically important oxides, as well as problems associated with applying surface science techniques to materials that can be insulating, the connection between the local structure of the reactive site and its activity and function had historically been based on indirect measurements performed on non-uniform powder catalysts. In addition, the extended single crystal surfaces that are easiest to prepare are the cleavage planes of the layered compounds α-MoO_3 and V_2O_5. The reactivity of these surfaces, however, can be dominated by a low density of highly reactive defect sites, thus limiting the utility of many surface science techniques to developing structure-reactivity relationships.[8,9]

This lack of detailed knowledge of how molecules adsorb and react on transition metal oxide surfaces and the evidence that the reactivity of these materials depended strongly on the local arrangement of atoms on the surface was the original motivation for the project. The approach was to take advantage of the PI's and collaborators' strengths in scanning tunneling microscopy (STM) to follow surface processes on the atomic level and epitaxial growth to synthesize suitable materials for such studies that are important to catalysis but difficult to obtain as the large single crystal typically required for such work.

The initial focus was on binary oxides of W and Ti; however, while the binary oxides can be active catalysts, addition of a second component often increases both reactivity and selectivity. For example, $FeMoO_4$ is more active for methanol oxidation to formaldehyde than MoO_3;[1,8] adding W to vanadia produces more active and selective catalysts for the selective catalytic reduction (SCR) of NO by NH_3,[10-12] and increases the selectivity of toluene oxidation to benzaldehyde;[13] vanadium pyrophosphate is a much more selective catalyst than vanadia for butane oxidation to maleic anhydride;[14,15] and vanadia-molybdena catalysts are more reactive and selective than either individual oxide for methanol oxidation to formaldehyde and ethane dehydrogenation to ethylene.[2,16] Further, an oxide support can also influence the activity and selectivity of oxide catalysts. In particular, catalysts supported on reducible oxides such as TiO_2 are often more active than either bulk oxide catalysts or

catalysts supported on more refractory oxides such as alumina and silica. The selective catalytic reduction of NO by NH_3 is again a good example. At low loadings, vanadia supported on TiO_2 is more active than bulk vanadia or vanadia supported on silica or alumina.[17] Another example is the selective oxidation of o-xylene to phthalic anhydride where vanadia supported on TiO_2 is uniquely selective.[18] Thus, the work branched out from binary oxides to ternary oxides and model oxide/oxide supported catalysts and finally to size effects in oxide clusters.

The following sections will provide summaries of several areas where substantial contributions were made to the understanding of transition metal oxide catalysis including: 1) oxidation and reduction mechanisms of tungsten oxide and their impact on catalytic reactions and pathways;[19-26] 2) the surface structure of anatase and its impact on reactivity;[21,27-31] 3) interactions between vanadia layers and titania supports and their implications on catalysis;[32-34] 4) size and support effects on the structure, reactivity and stability of Co oxide clusters.[35,36] This is not intended as an exhaustive list of the work done on the project, but rather as key examples of the most important findings.

2. Connecting Local Structure and Reactivity of a Binary Transition Metal Oxide – WO_3

The objectives of this effort were to understand how oxidation and reduction determine the types of sites available for reaction on a binary oxide surface and further to determine the importance of the accessibility and oxidation state of the metal cations and their proximity to bridging and terminal oxygen species to determining the catalytic pathway and activity. Tungsten oxide was chosen as the surface for these experiments because of its catalytic activity and its structure which allows the features mentioned above to be varied systematically.

Figure 1 shows a sequence of STM images that we obtained from a freshly cleaved WO_3 crystal as it was cycled through reduction and oxidation.[20] The cleaved surface exposed large terraces that appeared rough on an atomic scale as shown in Fig. 1.a. No changes were observed when the sample was heated in O_2 pressures above 10^{-4} torr, however, when the pressure was decreased to 10^{-5} torr the long range structure shown in Fig. 1.b was observed; this structure could be explained in terms of ordered arrays of W_6O_{18} clusters on the surface. After prolonged annealing (> 10 hrs) the clusters gave way to a well-ordered c(2×2) surface (Fig. 1.c). Reduction by annealing in UHV led to c(4×2), (2×2) and c(6×2) structures; the c(4×2) structure is shown in Fig. 1.d. Further reduction by preferential oxygen sputtering resulted in the (1×1) surface in Fig. 1.e. This sequence was reversible: at every stage the surface could be restored to the original, rough state by annealing in O_2 pressures above 10^{-4} torr as shown in Fig. 1.f.

The c(2×2) surface has been assigned to a WO_2 plane in which every other W atom is covered by a terminal O.[37] If all the W atoms are in a +6 oxidation state, this corresponds to the highest O coverage that yields a non-polar surface, thus this surface has been considered "fully oxidized." Decreasing the terminal O coverage to 1/4 accounts for the c(4×2) structure as well as the (2×2) and c(6×2) structures which differ only in the arrangement of the terminal O.[3] For these surfaces, maintaining charge neutrality dictates that 2/3 of the exposed W atoms be reduced to W^{5+}. The (1×1) structure has been assigned to a bare WO_2 plane with all the W ions reduced to W^{5+}.[2]

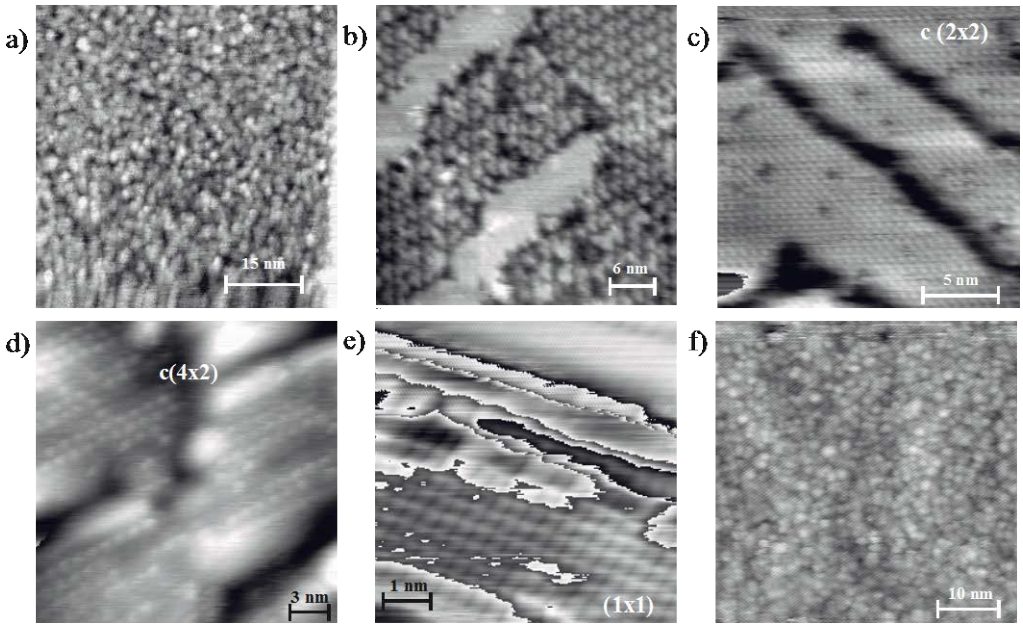

Figure 1. STM images of WO_3 (001) obtained after different surface treatments. (a) Cleaved in air and then annealed at 800 K in 10^{-4} torr O_2. (b) Annealed at 800 K in 3×10^{-5} torr O_2 for 2 hours. (c) After annealing at 800 K in 3×10^{-5} torr O_2 for 10 hours. (d) After 500 eV Ar^+ bombardment and annealing at 800 K in UHV. (e) After bombarding the surface in (d) with Ar^+ and annealing at 800 K in UHV. (f) After annealing the surface in (e) at 800 K in 10^{-4} torr O_2.

An intriguing aspect of the results is that the "fully oxidized" surface was only observed after decreasing the O_2 pressure. Phrased another way, the "fully oxidized" surface was prepared by reduction. This apparent contradiction could be understood in terms of bulk oxidation and reduction.[20] In this case, oxygen deficiency is accommodated partly by interstitial reduced cations. In an oxidizing environment the reduced ions segregate to the surface where they are oxidized; the disorder can be explained by the limited mobility of the newly formed WO_3 moieties on the surface at the annealing temperature. Reduction drives the excess W ions back into the bulk leaving a well-ordered c(2×2) surface behind. These results have important implications on catalysis. They show that although electron counting arguments are a good starting point for considering the sites available for reaction on an oxide surface, bulk oxidation and reduction, surface segregation, and surface diffusion must also be considered. Along the same lines, the surface reactivity cannot be anticipated solely from the surface structure and electron counting arguments which would predict that the c(2×2) surface would be unreactive towards oxygen.

The activity of the c(2×2) surface for dehydrogenation versus dehydration was characterized by studying the adsorption and reaction of the series of alcohols methanol, 1-propanol, 2-propanol, and t-butanol which are progressively easier to dehydrate.[19,38] Temperature programmed desorption results indicated that all the alcohols readily adsorb with some of the alcohol molecularly desorbing at 400 K. For the higher alcohols, only the dehydration products, propylene, i-butylene and water, were observed at higher temperatures indicating that the c(2×2) surface is only active for dehydration. The alkene desorption temperatures decreased in the series 1-propanol, 2-propanol, t-butanol indicating that C–O bond scission was the rate-limiting step. Consistent with this picture, methanol desorption products began to desorb at even higher temperatures, unfortunately the desorption temperature was too high to

complete the TPD trace without damaging the WO_3 crystal. Although an α–H must be abstracted during dehydration, since the rate is limited by breaking the C–O bond the rate is insensitive to whether the H is abstracted by a terminal or bridging oxygen. *Thus for alcohol dehydration on WO_3, the terminal oxygens are irrelevant.*

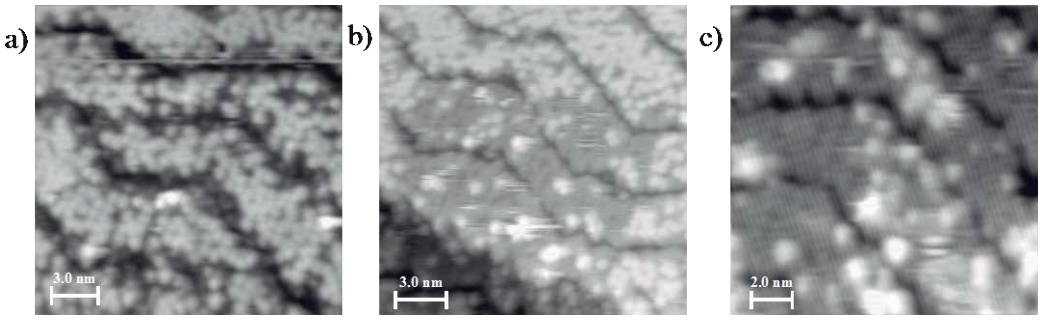

Fig. 2. STM images obtained after exposing c(2×2) WO_3(001) to 90 L of 1-propanol at 300 K and annealing to 400 K. (a) At high sample biases (3 V) the 1-propoxide appears as white spots. (b) Imaging at lower biases sweeps the 1-propoxide aside leaving the denuded area at the center of the image. (c) Zooming in on the denuded area reveals both the 1-propoxide and the c(2×2) substrate structure.

As illustrated in Fig. 2 the surface alkoxide intermediates in alcohol dehydration could be imaged following heating to desorb unreacted alcohol and some water. The images show that the alkoxide bonds to the terraces with no preference for steps or other defects. Further, the alkoxides could be removed from the surface by reducing the imaging bias. Under the same conditions the tip does not affect the WO_3 surfaces, thus moving the molecule aside reveals the structure of the underlying adsorption site. At lower coverages it could be shown that the bright features associated with the alkoxide appear between the O atoms in the c(2×2) structure, indicating that the alkoxide bonds to the exposed W^{6+} ions on the surface. Thus using STM together with TPD we have shown that the alcohols adsorb molecularly at 300 K and then dissociate to form an alkoxide at 400 K; that the alkoxides bond to exposed, coordinatively unsaturated W^{6+} ions on c(2×2) terraces; and that alkoxides in these sites only undergo dehydration reactions.[19] *Therefore it can be concluded that while exposed cations are required for dissociative adsorption, the cations need not be reduced.*[19]

We found that when WO_3 epitaxial films were gradually reduced between the structures with ¼ the surface W capped by terminal O (Fig. 1.d) and (1×1) surfaces with no terminal O (Fig. 1.e), a series of interesting striped structures were seen as highlighted in Fig. 3.[22-24,26] Figure 3 starts with a p(2×2) surface with ¼ ML of terminal oxygen and shows that as the surface is reduced at temperatures above 800 K, strands form on the surface that progressively move closer together until they merge to form flat (1x1) terraces with no terminal oxygen. Higher resolution images revealed a 2× periodicity along the strands and so as the surface is reduced the periodicity changes from p(5×2) to p(4×2) to p(3×2). Wide range images of the surfaces revealed a regular zigzag pattern of orthogonal p(*n*×2) and p(2×*n*) domains (*n* can be 3, 4, or 5) that could be understood in terms of equilibrating the stress induced by the uniaxial reconstruction.[23] We have performed a detailed study of the structure of the domain boundaries and the other characteristic defects that appear on these surfaces.[23] Based on an analysis of high-resolution, bias-dependent images and the heights of the strands, the strands were assigned to two W atom wide (1×1) terraces.[22] Terminal oxygen in the troughs give the structures a stoichiometry intermediate between the p(2×2) and (1×1) surfaces and a decreasing oxygen to W ratio in moving from p(5×2) to p(4×2) to p(3×2), consistent with observing these structures between the p(2×2) and

(1×1) structures and the strands moving closer together as the surface is reduced. The steps on the (1×1) surface in Figs. 3e,f are half the monatomic step height on WO_3 (100). These half-height steps can be associated with bulk shear planes intersecting the surface and thus are indicative of a change in the way the material responds to reduction from bulk migration of reduced cations to crystallographic shear.

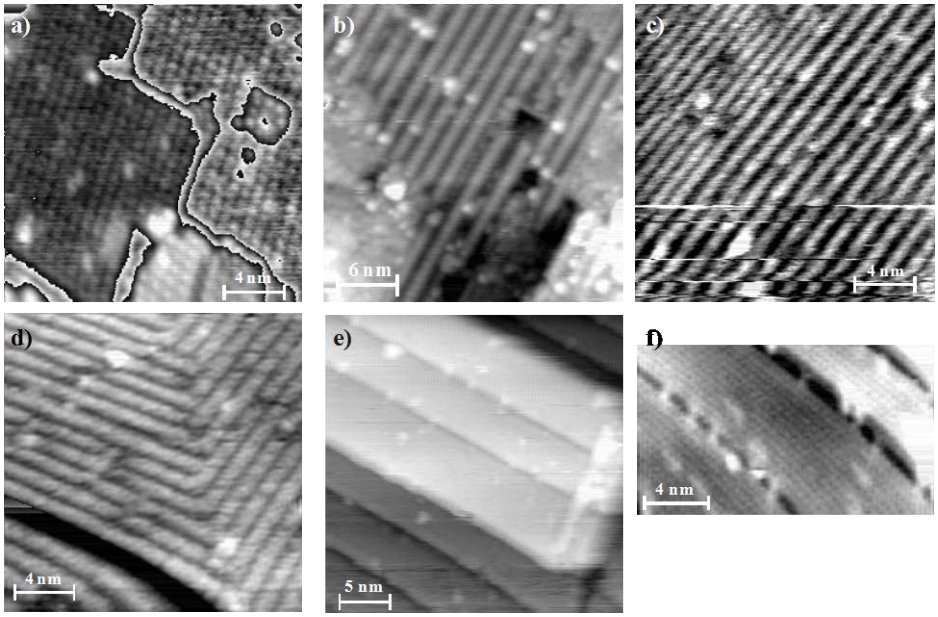

Figure 3. Sequence of unoccupied state STM images of a WO_3(100) thin film as it was progressively reduced by annealing at temperatures between 800 - 970 K in O_2 pressures less than $3x10^{-5}$ torr. The total annealing time in going from (a) to (e) was 10 hours. The surface periodicities are: (a) p(2×2), (b) p(5×2), (c) p(4×2) plus p(3×2), (d) p(3×2) plus p(2×3), and (e) (1×1). The image in (f) is a close-up of the surface in (e). The contrast in (a) and (f) were enhanced by cycling through the grayscale on each terrace.

To determine how the surface structures affect the reactivity and catalytic function of WO_3, the adsorption and reaction of 1-propanol was studied using temperature-programmed desorption (TPD) and STM.[25] We chose 1-propanol because it was the most difficult to dehydrate of the series of alcohols we had studied on stoichiometric *c*(2x2) WO_3(001),[19] and so if the structure shifted the activity from dehydration to dehydrogenation, we would most likely see this change for 1-propanol. Figure 4 shows a series of STM images recorded during exposure of a stranded p(*n*×2) surface to 1-propanol. The images show accumulation of bright dots solely on the tops of the strands, identifying the strands as the reactive sites. The images also show that once a molecule adsorbs on top of a strand, the adsorption rate at neighboring sites accelerates. As a result, with time some strands became fully occupied while others remained completely vacant. The STM image in Fig. 4f in which both the surface and adsorbate can be resolved shows that the adsorbates localize on top of the bright spots on top of the strands. These spots are associated with exposed W cations on the strands,[22] so this result is not surprising.

In the TPD experiments on the stranded surface, the only reaction products observed were propene and water, the same as c(2×2) WO_3 (001) and so the reduction and change in structure did not alter the catalytic pathway.[25] On the stranded surface, however, the propene desorbed at much lower temperatures. On surfaces where non-stoichiometric terminal oxygen structures coexisted with the

strands, a propene desorption peak appeared at temperatures intermediate between the stranded and stoichiometric c(2×2) surfaces; as the surface was reduced and became entirely covered by strands this intermediate peak disappeared. As detailed above, the propene desorption peaks on the c(2×2) surface are limited by the rate of C–O bond breaking and so the decrease in desorption temperature indicates a decrease in activation energy for C–O bond breaking. Because the non-stoichiometric terminal oxygen structures and the strands both expose W^{5+}, the large shift to lower temperatures on the stranded surface must be due in part to the surface structure. *Thus while the surface structure does not affect the acidic character of the WO_3 surface it does strongly affect reaction kinetics on the surface.*[25]

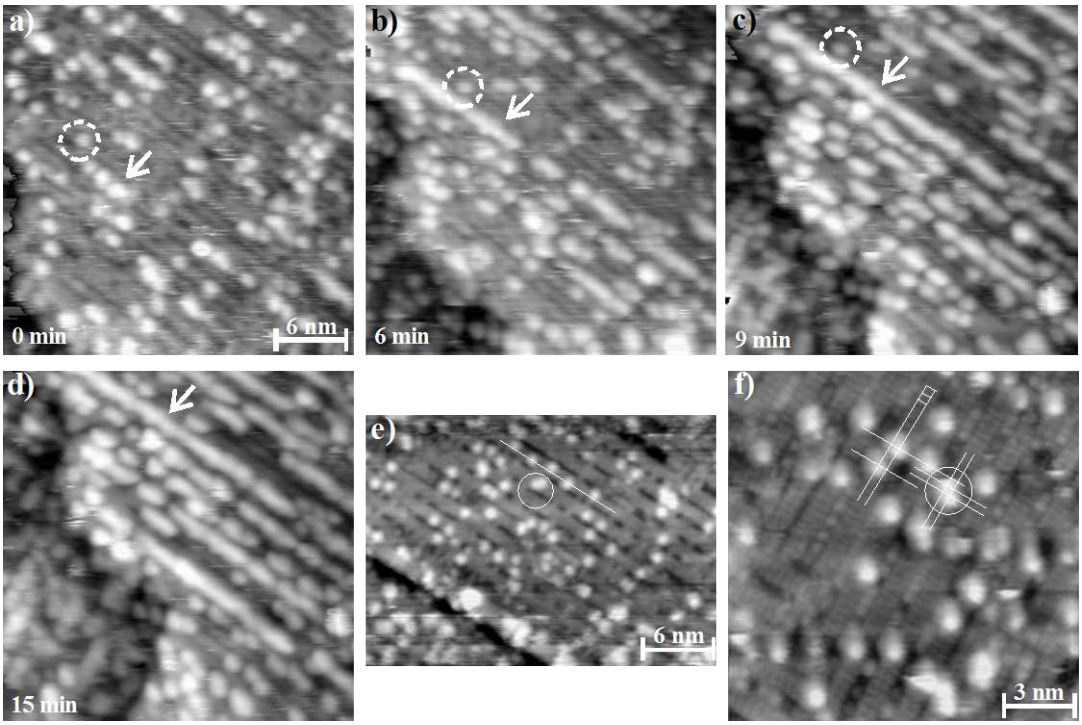

Figure 4. (a)-(d) Sequence of STM images recorded during exposure of the stranded p(*n*×2) WO_3 (100) surface to 5×10^{-7} torr 1-propanol at 300 K. The circle and arrow mark the same spot in all the images. Prior to recording the image in (a) the surface had already been exposed to a small dose of 1-propanol accounting for the adsorbates in the image. (e) After flashing the surface to the major propene TPD peak at 420 K, most of the adsorbates were removed. In this image we can also see that the adsorbates locate off-center on the strands. (f) High-resolution image showing both the adsorbates and the atomic structure of the strands. The grid shows that the adsorbates appear on top of the bright spots on the strands due to W atoms.

3. Structure and Reactivity of Anatase Surfaces

The structure and reactivity of the surfaces of the anatase polymorph of TiO_2 were studied as the catalytically relevant phase TiO_2 that had largely been ignored in the surface science literature due to the difficulty in obtaining suitable for detailed studies. This activity started as a collaboration with Yong Liang then at Pacific Northwest National Laboratory who was growing anatase phase films using molecular beam epitaxy (MBE) and also involved collaborations with Hiroshi Onishi in Japan and Robert Klie then at Brookhaven National Laboratory.

We found that the fully oxidized surfaces of anatase (001) exhibit a (4×1) reconstruction that is visible in STM and electron diffraction.[27] STM images of the surface show bright rows separated by 1.5 nm or 4×. The directions of the rows alternates across monatomic steps as shown in Fig. 5.a.

On vicinal single crystal surfaces, the steps preferentially aligned parallel to the 1× direction (Fig. 5.b), thus favoring double-height steps and suppressing one of the domains. Higher resolution images were obtained at lower biases and the image in Fig. 5.c shows the three rows of atoms between the bright rows. The non-contact atomic force microscopy (NC-AFM) image in Fig. 5.d also shows bright rows indicating that the rows are a topographical feature, thus the reconstruction can be considered to roughen the surface.[29] The unusual aspect of these results is that the fully oxidized, bulk-terminated (1×1) anatase surface is non-polar and thus the reconstruction is not driven by the need to create an autocompensated surface.

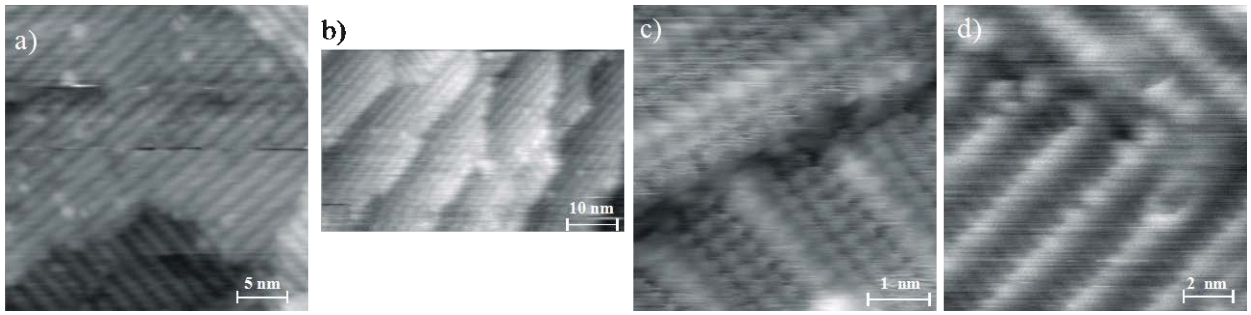

Figure 5. (a) STM image of an anatase (001) single crystal. The stripes are due to the (4×1) reconstruction; the crystal structure dictates that the direction of the stripes rotates by 90° when a single atom high step is decended. (b) On vicinal anatase (001), double height steps form, indicating that steps running parallel to the stripes are lower in energy. (c) Narrow range image showing atomic features in the trough. (d) The same corrugation is also seen in NC-AFM images.

We have studied carboxylic acid adsorption and reaction on (4×1) reconstructed and defective anatase surfaces using STM, NC-AFM, and TPD.[27-29,38] The carboxylic acids were chosen because the adsorption geometry has been well-characterized on the TiO_2 rutile surfaces,[39,40] and because a framework has been developed that relates the reaction products observed in TPD to the oxidation state and coordination of the surface Ti atoms.[41-43] Thus the imaging results provide the location of the Ti atoms while TPD work provides their oxidation state and coordination number.

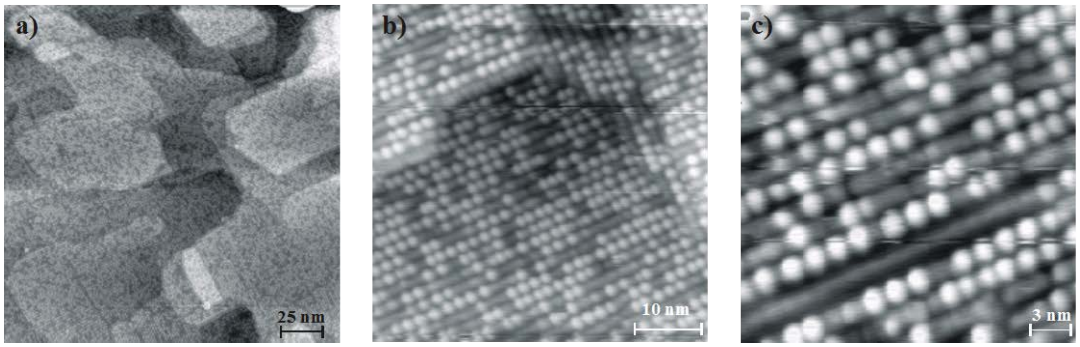

Figure 6. STM images at three different resolutions showing the anatase (001) after exposure to formic acid. The images were obtained after flashing to 850 K which improves the resolution but does not affect the location or spacing of the adsorbates. The bright spots on the tops of the rows only appeared after exposure to formic acids and thus can be attributed to formic acid or a decomposition product originating therefrom.

The STM images in Fig. 6 show that formic acid only adsorbs centered on top of the bright rows that define the (4×1) reconstruction; acetic acid behaves similarly.[28] In addition, the minimum distance between the molecules is 2×, consistent with formate bridging two exposed Ti atoms, the geometry seen on rutile surfaces. This is reinforced by our NC-AFM work that showed formate

centered between two bright spots on the crests of the rows.[29] These findings eliminated high index microfacet models since these place reactive four-fold coordinated Ti atoms either straddling the bright row or in the trough. In addition, NC-AFM images revealed corrugations much smaller than would be suggested by {101}-microfacet models. Thus, the imaging results were most consistent with an ad-molecule model proposed by Selloni and co-workers.[44] In this model, a raised, distorted TiO_2 group replaces a row of Ti and O atoms within the surface.

Although the ad-molecule model exposes four-fold coordinated Ti, the TPD results indicated that the reconstructed anatase surface behaved differently than other TiO_2 surfaces.[28] In marked contrast to rutile surfaces, the (4×1) surface very strongly held both formate and acetate and yielded only decomposition products at high temperatures. Disrupting the (4×1) reconstruction by ion bombardment was found to make the anatase (001) surface behave more like other TiO_2 surfaces. Further, sequences of STM, XPS, and TPD experiments after ion bombardment showed that dehydration activity attributed to five-fold coordinated Ti^{4+} on rutile surfaces declined as the size and perfection of the (4×1) domains increased. In addition, none of the bimolecular ketonization products typically attributed to four-fold coordinated Ti^{4+} were observed.[41-43] Thus carboxylates adsorbed on top of the (4×1) rows behave differently than those adsorbed on rutile surfaces, even though the coordination of the Ti atoms and the adsorbate bonding may be the same. The origin of this difference could be attributed to the nature of the Ti in the ad-molecule rows. Although the Ti is four-fold coordinated in this model, one of the empty coordination shells projects downward towards the bulk leaving it inaccessible for bonding which can account for the lack of bimolecular reaction products.[38,44]

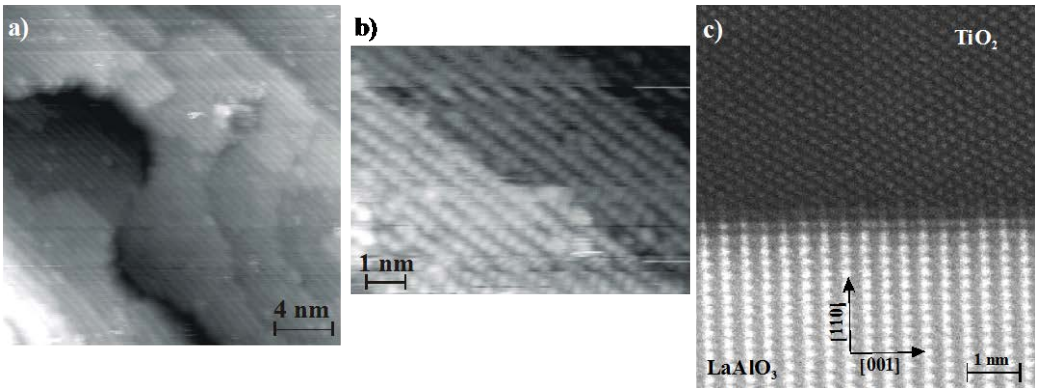

Figure 7. (a),(b) STM images of the surface of a TiO_2 film grown on $LaAlO_3$ (110). The row structure and the staggering of the atoms in adjacent rows in (b) yields the surface structure expected for anatase (101). (c) Cross-sectional STEM image of a TiO_2 film grown on $LaAlO_3$ (110). The pattern of Ti atoms at the top and their spacing can only be explained by anatase (102) planes parallel to the interface. The discrepancy between the bulk and surface structure was attributed to the surface faceting to expose more of the low energy (101) surface.

In addition to the anatase (001) surface, we were also able to show how films exposing the lowest energy anatase (101) surface that dominates the surface area of small crystallites could be fabricated.[30,32,45] It was anticipated that (101)-oriented anatase films could be grown on $LaAlO_3$(110) where the lattice match is nearly perfect along the $LaAlO_3$ [001] direction but there is a 4% mismatch along $LaAlO_3[1\bar{1}0]$. The TiO_2 films were deposited onto vicinal $LaAlO_3$(110) substrates to attempt to alleviate the lattice strain at the interface rather than in the bulk of the film. Surface characterization by RHEED, LEED, and STM all indicated epitaxial growth of anatase (101). The STM image in Fig.

7a shows steps and terraces with parallel rows. The atomic resolution image in Fig. 7b reveals the oblique primitive surface unit cell expected for anatase (101). In collaboration with Dr. Robert Klie of the Center for Functional Nanomaterials at Brookhaven National Laboratory, the films were also characterized using cross-sectional scanning transmission electron microscopy (STEM) coupled with electron energy loss spectroscopy (EELS).[30,31] The EELS spectra identified the bulk phase as anatase. A STEM image of the film and substrate is shown in Fig. 7c. The image shows that the film is epitaxial; however, the pattern at the top could only be explained by anatase (102) planes parallel to the interface. The surface data on the other hand were not consistent with anatase (102) surfaces. Anatase (102) can be thought of as vicinal to (101) with (101) terraces separated by (001) steps. As noted above, the (101) surface is the lowest energy surface. Thus, surface faceting to expose more of the low energy (101) terraces can explain the discrepancy between the surface and bulk characterization.

4. Interface Effects in Supported Oxide Catalysts

It has long been known that vanadia monolayers on TiO_2 supports are highly active and selective for a number of reactions including the partial oxidation of o-xylene to phthalic anhydride.[12,18] The structure of the vanadia monolayer had proven elusive and therefore we studied the growth and structure of vanadia on anatase with the goal of determining if the TiO_2 imparts distinct structural properties to the vanadia that increase its reactivity over bulk V_2O_5. We characterized the structural evolution of the vanadia layer during oxygen plasma assisted molecular beam epitaxy (OPA-MBE) using reflection high energy electron diffraction (RHEED), its surface structure using low energy electron diffraction (LEED) and STM following growth, its electronic structure using ultraviolet and x-ray photoelectron spectroscopy (UPS and XPS), and its bulk structure using x-ray diffraction (XRD) and transmission electron microscopy (TEM).[30-32] Following the structural characterization, we used TPD to compare the chemical properties of vanadia mono- and multilayers on anatase and rutile supports.[34] We started with the anatase (001) surface, using epitaxial films grown on $LaAlO_3$(100), which undergoes the (4×1) reconstruction discussed above and shown in the RHEED and LEED data in Fig. 8a,b. As soon as vanadia was deposited on the surface the 4x streaks in the LEED pattern faded. At 1 ML, the pattern became (1×1) as shown in Fig. 8c,d.[31,33] Below 600 K, XPS showed that the monolayer contained V^{5+}. At these lower temperatures, the RHEED pattern rapidly faded when the coverage was increased; XPS showed that these multilayers contained a mix of V^{5+} and V^{4+}. Above 700 K, however, the (1×1) RHEED pattern could be maintained ad infinitum as shown in Fig. 8d. At these high temperatures XPS showed only V^{4+} indicating that VO_2 grows pseudomorphically on anatase (001) *even though VO_2 is not known to crystallize in the anatase structure in the bulk.* Films grown at 775 K and cooled in the oxygen plasma exhibited the c(2×2) LEED pattern shown in Fig. 8e. This was attributed to oxygen adsorption on top of every other V atom on the surface which oxidizes all of the surface V atoms to 5+ in a manner analogous to the c(2×2) structure on WO_3{100} surfaces.[37] For a monolayer, such adsorption oxidizes all of the V to 5+. Thus the results indicate that the monolayer is unique in that it both adopts the substrate structure while maintaining the V^{5+} oxidation state.

To determine if the results were unique to anatase (001) surface, we looked at other anatase orientations. When a vanadia monolayer was deposited onto the anatase (101) terraces pictured in Fig. 7, little change in the surface structure was observed.[32] Characterization by XPS and UPS showed that

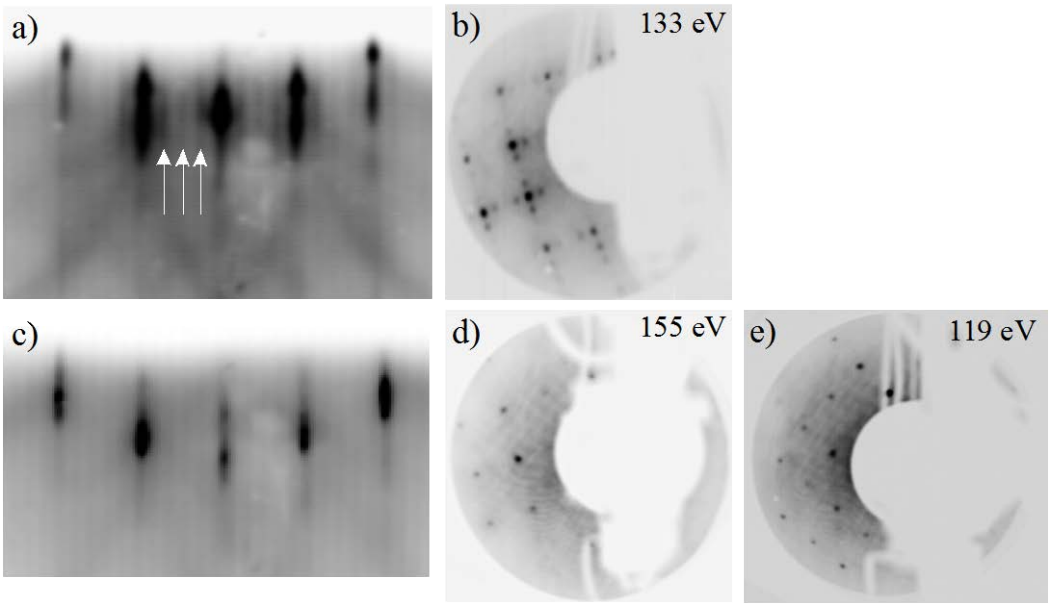

Figure 8. (a) RHEED pattern of anatase (001) thin film recorded along [100] zone axis, the arrows point to the ¼ order streaks due to the (4×1) reconstruction. (b) Corresponding (4x1) LEED pattern of the anatase (001) thin film. (c) RHEED pattern obtained after depositing 1 ML of vanadia onto the surface in (a) at 525 K; the ¼ order streaks have disappeared. (d) Corresponding (1×1) LEED pattern of the vanadia monolayer on anatase (001). (e) LEED pattern obtained after depositing 20 nm of VO_2 onto anatase (001) at 775 K, the periodicity is *c*(2×2).

the V in the monolayer was predominantly in the V^{5+} oxidation state. Thus, the monolayer behaves the same way on anatase (001) and (101) terraces – a pseudomorphic VO_2 layer forms with oxygen adsorption oxidizing the surface V to 5+. When the vanadia coverage was increased the RHEED pattern slowly faded. At the same time, V remained in the 5+ oxidation state and the Ti XPS peaks slowly attenuated. These results indicated that after the monolayer (which exhibited the expected V XPS peak intensity) was completed, 3D V_2O_5 clusters formed on the surface, again pointing to unique structural properties of the monolayer. The difference between the two anatase surfaces, however, was that it was not possible to maintain epitaxy on anatase (101), rather 3D vanadia clusters formed.[31-33] This difference may be related to the lower surface energy of the anatase (101) surface.

To determine if vanadia behaves similarly on other surfaces and to determine how the chemical properties of the substrate can affect the reactivity of the vanadia layer, we also studied vanadia deposition on WO_3(100) thin films. On the WO_3(100) (1×1) terraces in Fig. 3.e,f all of the W atoms are in the 5+ oxidation state. Thus it was expected that if we deposited vanadia onto an oxygen rich WO_3(100) surface, that it would adopt the (1×1) structure, with no terminal oxygen and all of the V would be in the 5+ oxidation state. This was in fact the case, starting with a p(2×2) surface with ¼ ML terminal oxygen the surface converted to (1×1) after depositing a vanadia monolayer. Reflection high energy electron diffraction movies recorded during vanadia deposition at 525 K showed that the 2× streaks began to fade immediately after opening the V shutter and the 1× streaks after the intensity of the 2× streaks fell to zero. Thus, similar to anatase, structural registry could not be maintained under conditions where V^{5+} forms, again highlighting the uniqueness of the monolayer in its ability to maintain all of the V in the 5+ oxidation state while adopting the structure of the substrate.

The results outlined above indicated that vanadia can adopt the structure of the support and that depending on the oxidation state of the cations in the support the surface vanadia can shift between 4+ and 5+ by adsorbing oxygen. This adsorption of oxygen to shift surface V from 4+ to 5+ was studied in more detail for vanadia layers on the rutile (110) surface of TiO_2.[34] For vanadia films on rutile (110) a series of surface phase transitions were observed depending on the oxygen pressure and temperature. When a vanadia film on rutile (110) was annealed at 925 K in 1×10^{-6} torr O_2, the LEED pattern in Fig. 9a was obtained; the pattern corresponds to a c(2×6) periodicity. When the oxygen pressure was dropped to 1×10^{-8} torr at 925 K, the (1×1) pattern in Fig. 9b was obtained; while increasing the pressure back to 1×10^{-6} torr caused spots due to longer range periodicities to begin to reappear (Fig. 9c). The cycling between the structures indicates that the patterns are associated with oxygen changing the surface. Finally, dropping the temperature to 725 K produced the (2×2) pattern seen in Fig. 9d. The oxygen-vanadium phase diagram indicates that the pressures and temperatures are within the range where VO_2 is the favored phase,[11] indicating that the structural changes are restricted to the surface and can be associated with oxygen adsorption oxidizing surface V to 5+, the oxidation state usually associated with catalytic vanadium oxides. The assignment of the different structures to VO_2 layers with different amounts of capping oxygen species was confirmed by ion scattering measurements.[34]

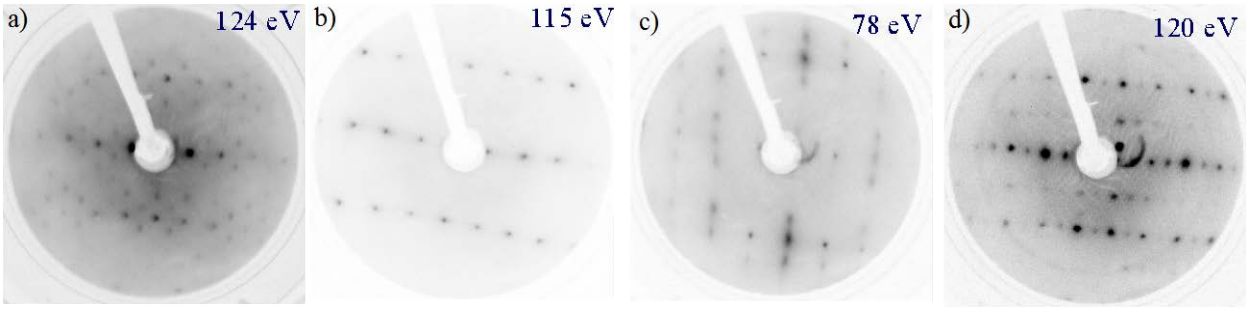

Figure 9. LEED patterns recorded after epitaxial VO_2 thin films on rutile (110) were subjected to different oxygen treatments. (a) 1×10^{-6} torr O_2 at 925 K for 1 hr; (b) 1×10^{-8} torr O_2 at 925 K for 1 hr; (c) surface in (b) exposed to 1×10^{-6} torr O_2 at 925 K ; and (d) 1×10^{-6} torr 725 K.

Alcohol TPD was used to distinguish electronic and structural effects in determining the catalytic properties of supported transition metal oxide layers, specifically vanadia. A key question we sought to address was does a vanadia monolayer on TiO_2 behave chemically similar to the surface of a vanadia multilayer with the same surface structure and oxidation state? To answer this question we compared 1-propanol temperature programmed desorption (TPD) results for vanadia monolayers and multilayers with the same structure; the results are shown in Fig. 10 for a rutile (110) structured TiO_2 substrate.[34] Figure 10a shows the TPD results for 0.7 ML of vanadia following growth where V^{5+} predominates. The 1-propanol desorption above 500 K is consistent with adsorption on uncovered areas of the rutile substrate;[46] while the peaks just above 400 K can be associated with the vanadia. Repeating the TPD experiment without reoxidizing the vanadia (Fig. 10b) causes the desorption peaks to shift to higher temperatures. The shift can be associated with reduction of the surface caused by oxidation of the 1-propanol,[47] as evidenced by the strong bandgap emission in the UPS spectrum in Fig. 10d acquired after the TPD experiment. Not surprisingly, as shown in Fig. 10c, the high temperature peaks due to the rutile substrate are suppressed for epitaxial vanadia multilayers. More

interestingly, the lower temperature propionaldehyde peak associated with the vanadia persists with little change. The only significant difference is an increase in unreacted 1-propanol desorption. This is markedly different from the inactivity reported for bulk-structured V_2O_5.[48] Thus a couple of important conclusions could be drawn from these results: 1) Ti–O–V bonds are not required for vanadia to be active for alcohol dehydrogenation; and 2) as long as the TiO_2 structure can be maintained as we move away from the vanadia/titania interface, the vanadia can be active. This suggests that at least for vanadia/titania, structural promotion is more important than electronic effects.

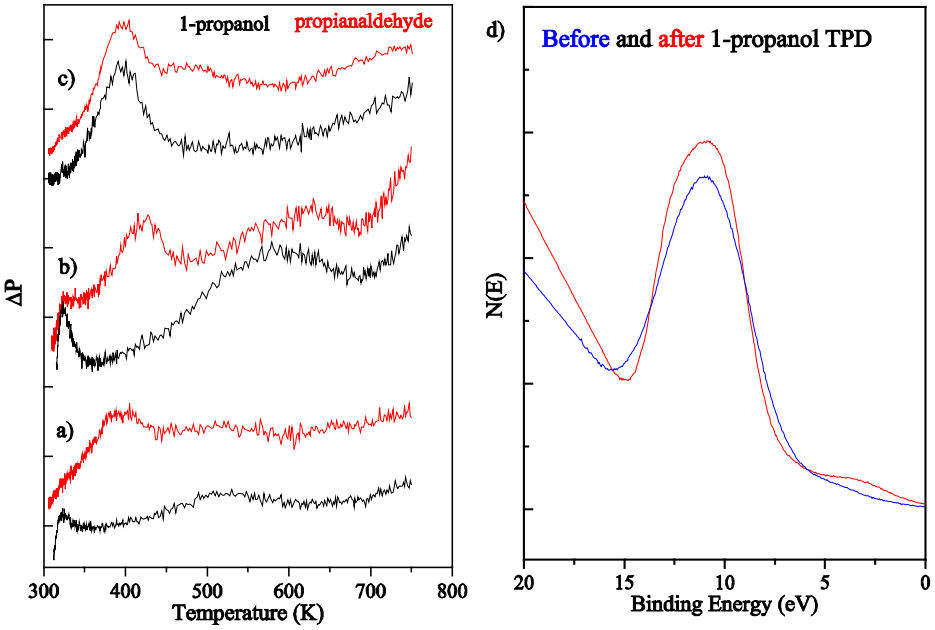

Figure 10. (a) - (c) Saturation exposure 1-propanol TPD curves for (a) 0.7 ML vanadia on rutile (110) following growth, (b) second 1-propanol exposure to the film in (a) without reoxidation, and (c) a 12 nm thick vanadia film on rutile (110) following growth. (d) He II UPS spectra recorded before (blue) and after (red) the TPD experiment in (a).

To determine how the structure of the vanadia layers affects their reactivity, the results described above were compared with those obtained for epitaxial vanadia layers grown on anatase (001). Similar to the rutile substrate, there was not much change in the 1-propanol and propionaldehyde desorption peaks when the vanadia thickness was changed. In comparison to the rutile-structured substrate, however, far less propionaldehyde was formed on the anatase substrate where most of the 1-propanol desorbed unreacted. Table 1 provides a comparison of the difference between the reaction pathway for adsorbed 1-propanol on different vanadia thicknesses on rutile (110) and anatase (001). The table shows that more

Substrate	Thickness (nm)	C_3H_6O / n-C_3H_7OH
Rutile	0.24 (0.75 ML)	1.17
Rutile	1.0	0.12
Rutile	11.7	0.14
Rutile	16.2	0.12
Anatase	0.10	0.07
Anatase	0.30	0.07
Anatase	1.0	0.06
Anatase	20	0.08

Table 1. Ratio of propionaldehyde to 1-propanol desorption as a function of VO_x thickness for anatase and rutile substrates.

than half the adsorbed propanol reacted in the monolayer regime for vanadia on rutile (110) while all the other surfaces oxidized only 5 – 10% of the adsorbed alcohol.

The differences between the vanadia sub-monolayer on rutile (110) and anatase (100) could be linked to the types of defects on the two TiO_2 surfaces. The common defects on rutile (110) are oxygen vacancies that are active for alcohol deprotonation, the first step in the oxidative dehydrogenation of alcohols and thus can assist the oxidation reaction.[46,49,50] In contrast, the most common defects seen in STM image of anatase (001) and (101) surfaces are dim spots or apparent missing Ti atoms.[51-54] These dim spots are due to water and oxygen vacancies are rare on these surfaces,[55,56] suggesting that the anatase surface lacks sites that can assist alcohol dehydrogenation.

5. Support and Size Effects in the Stability, Structure, and Reactivity of Co Oxide Clusters

Work on Co oxide nanoclusters was motivated by reports that Co oxides and Co-containing oxides are catalytically active and selective for a wide range of important reactions that typically require Pt group metals.[57-65] Cobalt oxide catalysis is sensitive to just about every effect seen in heterogeneous catalysis including particle size and support effects.[60,66-69] Therefore, as part of this effort we sought to uncover the intrinsic factors that govern the reactivity of Co oxides nanoclusters using STM augmented by other methods, including AP-XPS at Brookhaven National Laboratory (BNL).

The most surprising finding of this effort was that even weakly interacting supports could dramatically impact the stability of the different Co oxide phases and the shape of the Co oxide clusters.[36,70] Specifically, work on Co oxide on Au(111) indicated that high surface energy supports dramatically shift the equilibrium between CoO and Co_3O_4 to CoO as the size of the supported particles decreases.[36] Thus smaller particles become more difficult to oxidize than larger ones, the opposite of the usual expectation.

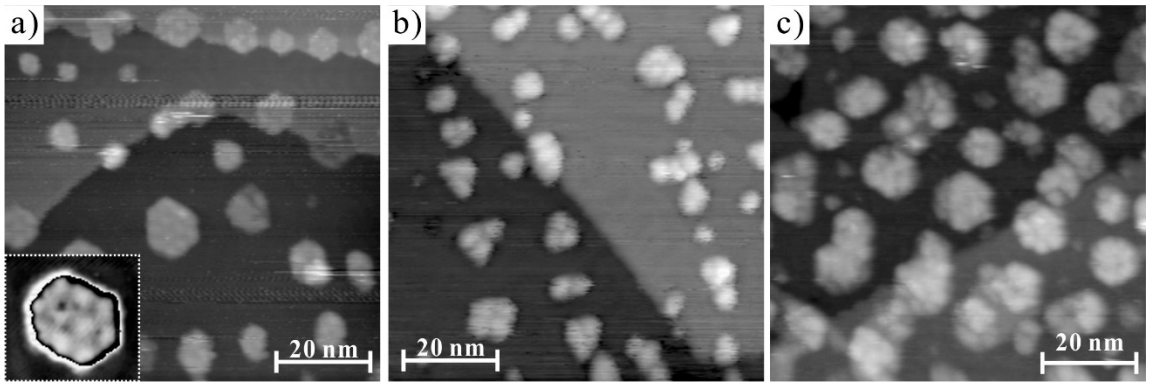

Figure 11. STM images of cobalt oxide grown on Au(111): a) 0.2 ML; b) 0.4 ML; c) 1.0 ML. The inset in (a) highlights the internal structure of one of the clusters. Despite the coverage doubling between (a) and (b), the average cluster area and the cluster density are nearly unchanged.

As summarized in Fig. 11, Co oxide growth under conditions where Co_3O_4 is thermodynamically favored on Au(111) proceeds two dimensionally up to 0.2 ML and then switches to three dimensional growth.[36] This leads to little difference between 0.2 ML and 0.4 ML Co oxide in terms of the fraction of the surface covered and the average cluster area. On the other hand, the clusters in Figs. 11b and 11c are roughly twice as high as those in 11a, consistent with a switch from monolayer to bilayer growth. The clusters in Figs. 11b and 11c also show line defects absent from the clusters in Fig. 11a. Instead the cluster surfaces at the lower coverage are dominated by a hexagonal superstructure

consistent with the lattice mismatch between CoO and Au(111) (inset Fig. 11a); this pattern is not seen at the higher coverages suggesting that Co_3O_4, which is perfectly lattice matched to Au(111), forms. Photoelectron spectroscopy measurements confirmed a phase transition from CoO to Co_3O_4 with increasing coverage or cluster size.

This size dependent phase transition from CoO to Co_3O_4 under conditions where Co_3O_4 is favored in the bulk was explained in terms of the differences in the CoO rock salt and Co_3O_4 spinel structures and the higher surface energy of the support versus the oxide.[36] Along [111] the rock salt structure repeat unit consists of alternating hexagonal Co and O planes. While the O planes in the spinel are also hexagonal, the spinel alternates between two distinct Co layers. As a result, the thinnest (111) CoO layer contains one Co and one O plane while Co_3O_4 requires at least two oxygen and two Co layers. This is consistent with the rough doubling of the height from Fig. 11a to 11b when Co_3O_4 formed. The end result is that oxidizing CoO to Co_3O_4 increases the exposure of the high surface energy substrate while also increasing the occupation of high energy edge and corner sites, thereby making oxidation less favorable. An analytic expression based on the surface and interfacial energies and the densities of the different oxide phases was developed that captures the variation in the free energy of oxidation with cluster size. Plugging in literature estimates of the surface energies of Co oxides suggested that at the 670 K growth temperature the dissociation pressure of Co_3O_4 on Au(111) can increase from 7.5×10^{-13} to 3.9×10^{-7} torr. Since Co oxide phases display markedly different reactivities, this can help explain size and support dependent reactivity.

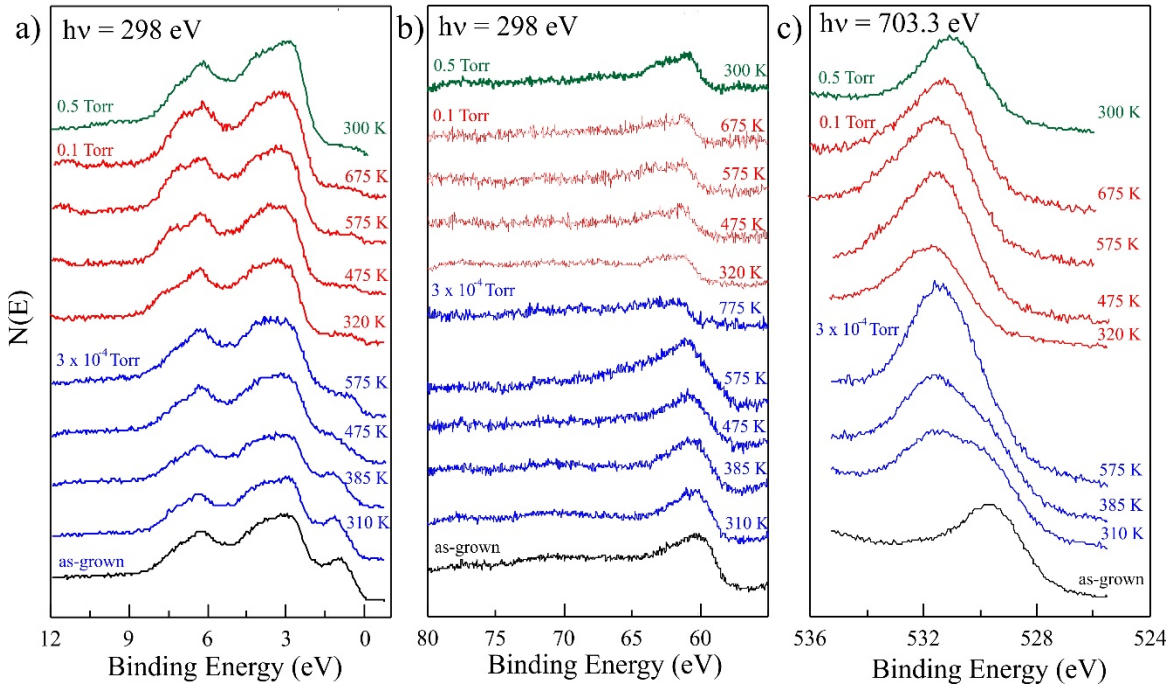

Figure 12. AP-XPS data for CoO_x/Au(111), a) valence band, b) Co 3p and c) O 1s regions. Starting with 1 ML Co_3O_4, the sample was heated to 775 K in 3×10^{-4} torr O_2 (blue), then at 775 K the O_2 pressure was increased to 0.1 torr (red) and the sample cooled to 300 K, then the O_2 pressure was increased to 0.5 torr (green).

Ambient pressure XPS (AP-XPS) experiments at BNL were carried out to monitor the chemical state of the Co during CO oxidation and to attempt to quantify the change in stability of the oxide phases at small cluster size; results for the latter are provided in Fig. 12. The first peak below E_F in the valence band spectra can be associated with Co_3O_4;[71] its loss of intensity on heating suggests

reduction towards CoO in 3×10^{-4} torr even at 575 K where the dissociation pressure of bulk Co_3O_4 is less than 10^{-13} torr.[72] Curiously, at the same time both the Co 3p and O 1s peaks shift to higher binding energies (the Co 3p peaks were characterized rather than the more typical and intense 2p peaks because the maximum photon energy on the beam line at NSLS I was insufficient to emit electrons from Co 2p levels). Finally, heating to 775 K causes a dramatic decline in the Co 3p peak intensity which can be related to CoO dissociation and the remaining Co migrating into the bulk.[36,70] Increasing the O_2 pressure at this point did not restore the Co peak intensity or cause the core level peaks to shift back to their original positions, though a small downward shift could be seen. While a shift of the Co 3p peaks to higher binding energy would suggest a higher oxidation state, we find that the gap between the O 1s and Co 3p peaks increases on heating. The shift in the O 1s peak cannot be due to adsorbed O which would tend to decrease with increasing temperature, as would peaks due to adsorbed H_2O or OH groups. Rather the shift of both core levels together can be explained by the emergence of a band offset between the Co oxide and Au substrate due to an interfacial dipole. Such a dipole would arise from organization of the Co oxide into a plane of negatively charged O at the interface topped by a plane of positively charged Co and image charges in the Au. The dipole would shift the Co and O binding energies downward but not the Au which is grounded to the spectrometer. When this effect is taken into account, the position of the Co 3p peaks with respect to the O 1s peak is consistent with CoO and the valence band data. The loss of Co from the surface leads to smaller Co oxide clusters which then cannot be oxidized to Co_3O_4 even at 0.5 torr. Thus the in situ data suggest a decrease in the dissociation pressure of the larger Co_3O_4 clusters approaching nine orders of magnitude while the smaller clusters could not be oxidized at pressures another three orders of magnitude higher.

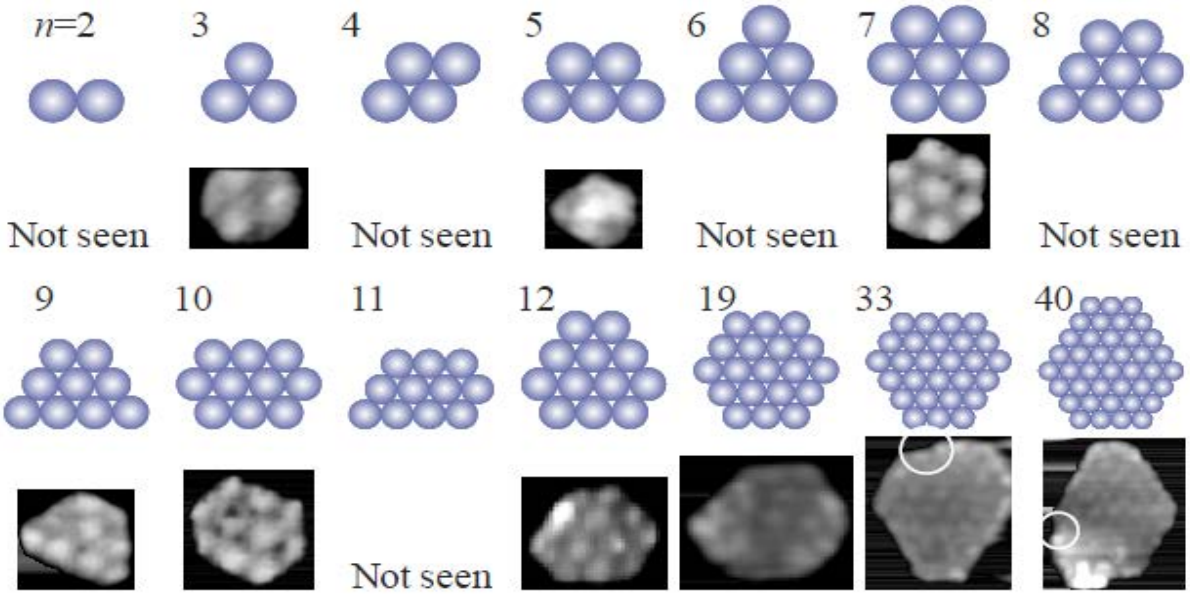

Figure 13. Evolution of CoO island shapes as a function of the number of bright spots (n) in the superstructure. The shaded balls represent the expected shapes based on close packed spheres. The STM images show the observed shape. The white circles highlight kinks resolved in the cluster edges for n = 33 and 40.

The lattice mismatch between CoO and Au was found to dramatically affect CoO island sizes and stabilities.[70] Equilibrium island shapes are determined by edge energies, for [111]-oriented rock salt islands asymmetric hexagonal shapes are favored due to the different energies of the alternating {100} and {111} edges. This assumes that the islands are large enough that the continuum description

of the edges applies. For islands with just a few atoms, this breaks down and the shape and stability of the islands varies strongly with size. For example, regular hexagons of seven atoms are far more stable than six or eight atom clusters.[73,74] For CoO on Au(111) we found that the equilibrium shape expected for rock salt (111) islands is not reached until the islands contained thousands of atoms.[70] Despite the modest rumpling of the surface due to the lattice mismatch, ≈0.15 Å, the bright spots in the superstructure replace the Co-O units as the fundamental unit that determines the shape and stability of the CoO islands; each unit cell of the superstructure contains 110 Co atoms. Figure 13 summarizes how the island shapes vary with the number of superstructure spots. The evolution of the shapes mimics that expected by the efficient close packing of spheres, and we find that upwards of 30 superstructure spots, or over 3,000 Co atoms, are required to see the favored asymmetric hexagonal shape. The results then highlight how even a weak interaction (insufficient to strain CoO from its bulk lattice constant) that results solely from geometric mismatch impacts the shape of supported clusters.

It was also found that the particle shape, which determines the occupancy of the {100} and {111} island edges, affects the reactivity of the CoO islands towards oxygen; thus the weak interaction of CoO with the Au substrate is sufficient to impact reactivity.[70] As illustrated in Fig. 14.a, once the CoO islands are large enough to be oxidized, the resulting Co_3O_4 clusters display characteristic "Y" defects. These defects are due to: the doubling of the in-plane periodicity in going from CoO to Co_3O_4; and oxidation initiated at specific edges of hexagonal CoO islands. Rearranging the 194 Co atom CoO cluster in Fig. 14b into the Co_3O_4 structure starting at the edges pointed to by the arrows, yields the three domain boundaries in Fig. 14.c when the growth fronts merge. In contrast, initiating oxidation on the top surface would yield random domain boundaries while if the edges were equally reactive the clusters would have six domain boundaries.

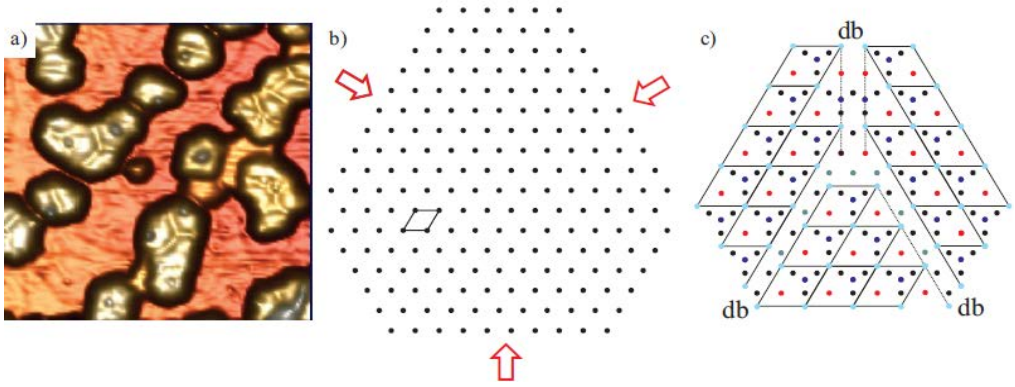

Figure 14. a) Three-dimensional rendering of an STM image of Co_3O_4 clusters on Au(111). The clusters all show line defects, typically in a Y configuration. b) Model of the Co atom arrangement in a 194 Co atom [111]-oriented island. The black line highlights the unit cell. The red arrows indicate the directions from which the Co atoms were rearranged to generate the Co_3O_4 cluster in c). In c), black represents Co atoms in the octahedral layer, light cyan Co in octahedral sites in the mixed octahedral/tetrahedral layer, red and blue Co in upper and lower tetrahedral sites, and dark cyan atoms at domain boundaries (db) that could not be fit into Co_3O_4 sites. The solid and dashed lines indicate unit cells and dbs respectively.

References

[1] C. J. Machiels, W. H. Cheng, U. Chowdry, W. E. Farneth, F. Hong, E. M. McCarron, and A. W. Sleight. *The effect of the structure of molybdenum oxides on the selective oxidation of methanol.* Applied Catalysis **25**, 249 (1986).

[2] M. Kennedy, A. Sexton, B. Kartheuser, E. M. G. Coda, J. B. McMonagle, and B. K. Hodnett. *Selective oxidation of methane to formaldehyde. Comparison of the role of promoters in hydrocarbon rich and lean conditions.* Catalysis Today **13**, 447 (1992).

[3] D. Gazzoli, A. Marucci, G. Mattei, M. Valigi, and R. J. Dragone. *Characterization of the zirconia-supported tungsten oxide system by laser Raman and diffuse reflectance spectroscopies.* Journal of Physical Chemistry B **101**, 11129 (1997).

[4] G. Busca, L. Lietti, G. Ramis, and F. Berti. *Chemical and mechanistic aspects of the selective catalytic reduction of NO_x by ammonia over oxide catalysts: A review.* Applied Catalysis B-Environmental **18**, 1 (1998).

[5] J. M. Tatibouet. *Methanol oxidation as a catalytic surface probe.* Applied Catalysis A:General **148**, 213 (1997).

[6] J. M. Tatibouët, J. E. Germain, and J. C. Volta. *Structure sensitive catalytic oxidation: alcohols on graphite-supported molybdenum trioxide.* Journal of Catalysis **82**, 240 (1983).

[7] A. Michalak, K. Hermann, and M. Witko. *Reactive oxygen sites at MoO_3 surfaces: ab initio cluster model studies.* Surface Science **366**, 323 (1996).

[8] U. Chowdry, A. Ferretti, L. E. Firment, C. J. Machiels, F. Ohuchi, A. W. Sleight, and R. H. Staley. *Mechanism and surface structural effects in methanol oxidation over molybdates.* Applications of Surface Science **19**, 360 (1984).

[9] K. B. Lewis, S. T. Oyama, and G. A. Somorjai. *TPD studies of vanadium oxide films deposited on gold.* Applied Surface Science **52**, 241 (1991).

[10] J. P. Chen and R. T. Yang. *Role of WO_3 in mixed V_2O_5–WO_3/TiO_2 catalysts for selective catalytic reduction of nitric oxide with ammonia.* Applied Catalysis A: General **80**, 135 (1992).

[11] L. Lietti, J. Svachula, P. Forzatti, G. Busca, G. Ramis, and F. Bregani. *Surface and catalytic properties of vanadia-titania and tungsta-titania systems in the selective catalytic reduction of nitrogen oxides.* Catalysis Today **17**, 131 (1993).

[12] M. D. Amiridis, R. V. Duevel, and I. E. Wachs. *Effect of metal oxide additives on the activity of V_2O_5/TiO_2 catalysts for the selective catalytic reduction of nitric oxide by ammonia.* Applied Catalysis B-Environmental **20**, 111 (1999).

[13] Z. Yan and S. L. T. Andersson. *Catalytic Oxidation of toluene over V_2O_5–WO_3 Catalytsts.* Applied Catalysis **66**, 149 (1990).

[14] G. J. Hutchings. *Vanadium phosphorus oxide catalysts for the selective oxidation of n-butane to maleic anhydride.* Catalysis Today **16**, 139 (1993).

[15] K. E. Birkeland, S. M. Babitz, G. K. Bethke, H. H. Kung, G. W. Coulston, and S. R. Bare. *Supported VPO catalysts for selective oxidation of butane. II. Characterization of VPO/SiO_2 catalysts.* Journal of Physical Chemistry B **101**, 6895 (1997).

[16] R. Burch and R. Swarnakar. *Oxidative dehydrogenation of ethane on vanadium-molybdenum oxide and vanadium-niobium-molybdenum oxide catalysts.* Applied Catalysis **70**, 129 (1991).

[17] M. D. Amiridis and J. P. Solar. *Selective catalytic reduction of nitric oxide by ammonia over V_2O_5/TiO_2, $V_2O_5/TiO_2/SiO_2$, and V_2O_5-WO_3/TiO_2 catalysts: effect of vanadia content on the activation energy.* Industrial & Engineering Chemistry Research **35**, 978 (1996).

[18] G. C. Bond. *What limits the selectivity attainable in the catalysed oxidation of o-xylene to phthalic anhydride?* Journal of Chemical Technology & Biotechnology **68**, 6 (1997).

[19] R. E. Tanner, P. Meethunkij, and E. I. Altman. *Identification of alcohol dehydration sites on an oxide surface by scanning tunneling microscopy.* Journal of Physical Chemistry B **104**, 12315 (2000).

[20] R. E. Tanner and E. I. Altman. *Effect of surface treatment on the γ-WO_3(001) surface: A comprehensive study of oxidation and reduction by scanning tunneling microscopy and low-energy electron diffraction.* Journal of Vacuum Science & Technology A **19**, 1502 (2001).

[21] E. I. Altman and R. E. Tanner. *Using scanning tunneling microscopy to characterize adsorbates and reactive intermediates on transition metal oxide surfaces.* Catalysis Today **85**, 101 (2003).

[22] M. Li, E. I. Altman, A. Posadas, and C. H. Ahn. *The p(4 x 2) surface reconstruction on epitaxial WO3 thin films.* Surface Science **542**, 22 (2003).

[23] M. Li, E. I. Altman, A. Posadas, and C. H. Ahn. *Surface phase transitions and related surface defect structures upon reduction of epitaxial WO_3(100) thin films: A scanning tunneling microscopy study.* Journal of Vacuum Science & Technology A **22**, 1682 (2004).

[24] M. Li, E. I. Altman, A. Posadas, and C. H. Ahn. *Surface phase transitions upon reduction of epitaxial WO_3 (100) thin films.* Thin Solid Films **446**, 238 (2004).

[25] M. Li, W. Gao, A. Posadas, C. H. Ahn, and E. I. Altman. *Reactivity of 1-propanol on p(n x 2) reconstructed WO_3(100) thin films.* Journal of Physical Chemistry B **108**, 15259 (2004).

[26] M. Li, A. Posadas, C. H. Ahn, and E. I. Altman. *Scanning tunneling microscopy study of terminal oxygen structures on WO3(100) thin films.* Surface Science **579**, 175 (2005).

[27] Y. Liang, S. P. Gan, S. A. Chambers, and E. I. Altman. *Surface structure of anatase TiO2(001): Reconstruction, atomic steps, and domains.* Physical Review B **63** (2001).

[28] R. E. Tanner, Y. Liang, and E. I. Altman. *Structure and chemical reactivity of adsorbed carboxylic acids on anatase TiO_2(001).* Surface Science **506**, 251 (2002).

[29] R. E. Tanner, A. Sasahara, Y. Liang, E. I. Altman, and H. Onishi. *Formic acid adsorption on anatase TiO_2(001)-(1x4) thin films studied by NC-AFM and STM.* Journal of Physical Chemistry B **106**, 8211 (2002).

[30] W. Gao, R. Klie, and E. I. Altman. *Growth of anatase films on vicinal and flat $LaAlO_3$ (110) substrates by oxygen plasma assisted molecular beam epitaxy.* Thin Solid Films **485**, 115 (2005).

[31] W. Gao, M. Li, R. Klie, and E. I. Altman. *Growth and characterization of model oxide catalysts.* Journal of Electron Spectroscopy and Related Phenomena **150**, 136 (2006).

[32] W. Gao and E. I. Altman. *Growth and structure of vanadium oxide on anatase (101) terraces.* Surface Science **600**, 2572 (2006).

[33] W. Gao, C. M. Wang, H. Q. Wang, V. E. Henrich, and E. I. Altman. *Growth and surface structure of vanadium oxide on anatase(001).* Surface Science **559**, 201 (2004).

[34] M. Li and E. I. Altman. *Reactivity of Epitaxial Vanadia on TiO_2: Are Support Interactions Required for Reactivity?* Journal of Physical Chemistry C **113**, 2798 (2009).

[35] M. Li and E. I. Altman. *Shape, Morphology, and Phase Transitions during Co Oxide Growth on Au(111).* Journal of Physical Chemistry C **118**, 12706 (2014).

[36] M. Li and E. I. Altman. *Cluster-size dependent phase transition of Co oxides on Au(111).* Surface Science **619**, L6 (2014).

[37] F. H. Jones, K. Rawlings, J. S. Foord, R. G. Egdell, J. B. Pethica, B. M. R. Wanklyn, S. C. Parker, and P. M. Oliver. *An STM study of surface structures on $WO_3(001)$.* Surface Science **359**, 107 (1996).

[38] E. I. Altman and R. E. Tanner. *Using scanning tunneling microscopy to characterize adsorbates and reactive intermediates on transition metal oxide surfaces.* Catalysis Today **85**, 101 (2003).

[39] H. Onishi and Y. Iwasawa. *STM-imaging of formate intermediates adsorbed on a TiO_2 (110) surface.* Chemical Physics Letters **226**, 111 (1994).

[40] K. I. Fukui, H. Onishi, and Y. Iwasawa. *Imaging of individual formate ions adsorbed on TiO_2 (110) surface by non-contact atomic force microscopy.* Chemical Physics Letters **280**, 296 (1997).

[41] K. S. Kim and M. A. Barteau. *Pathways for carboxylic acid decomposition on TiO_2.* Langmuir **4**, 945 (1988).

[42] K. S. Kim and M. A. Barteau. *Structural dependence of the selectivity of formic acid decomposition on faceted $TiO_2(001)$ surfaces.* Langmuir **6**, 1485 (1990).

[43] K. S. Kim and M. A. Barteau. *Structure and composition requirements for deoxygenation, dehydration and ketonisation reactions of carboxylic acids on $TiO_2(001)$ single-crystal surfaces.* J. Catal. **125**, 353 (1990).

[44] M. Lazzeri and A. Selloni. *Stress-Driven Reconstruction of an Oxide Surface: The Anatase TiO_2 (001)-1x4 Surface.* Physical Review Letters **87**, 266105 (2001).

[45] M. Lazzeri, A. Vittadini, and A. Selloni. *Structure and energetics of stoichiometric TiO_2 anatase surfaces.* Phys. Rev. B **63**, 155409 (2001).

[46] E. Farfan-Arribas and R. J. Madix. *Role of Defects in the Adsorption of Aliphatic Alcohols on the $TiO_2(110)$ Surface.* J. Phys. Chem. B **106**, 10680 (2002).

[47] G. S. Wong, M. R. Concepcion, and J. M. Vohs. *Oxidation of Methanol to Formaldehyde on Vanadia Films Supported on $CeO_2(111)$.* J. Phys. Chem. B **106**, 6451 (2002).

[48] T. Feng and J. M. Vohs. *Temperature-Programmed Desorption Study of the Selective Oxidation of Alcohols on Silica-Supported Vanadium Oxide.* J. Phys. Chem. B **109**, 2120 (2005).

[49] Z. Zhang, R. Rousseau, J. Gong, S.-C. Li, B. D. Kay, Q. Ge, and Z. Dohnalek. *Vacancy-Assisted Diffusion of Alkoxy Species on Rutile $TiO_2(110)$.* Physical Review Letters **101**, 156103 (2008).

[50] L. J. Burcham, L. E. Briand, and I. E. Wachs. *Quantification of active sites for the determination of methanol oxidation turn-over frequencies using methanol chemisorption and in situ infrared techniques. 1: Supported metal oxide catalysts.* Langmuir **17**, 6164 (2001).

[51] W. Gao, R. Klie, and E. I. Altman. *Growth of Anatase Films on Vicinal and Flat $LaAlO_3$ (110) Substrates by Oxygen Plasma Assisted Molecular Beam Epitaxy.* Thin Solid Films **485**, 115 (2005).

[52] R. E. Tanner, E. I. Altman, A. Sasahara, H. Onishi, and Y. Liang. *Formic acid adsorption on anatase TiO_2(001)-(1 × 4) thin films studied by NC-AFM and STM.* Journal of Physical Chemistry B **106**, 8211 (2002).

[53] R. E. Tanner, Y. Liang, and E. I. Altman. *Structure and chemical reactivity of adsorbed carboxylic acids on anatase TiO_2(001).* Surface Science **506**, 251 (2002).

[54] Y. Liang, S. Gan, S. A. Chambers, and E. I. Altman. *Surface structures of anatase TiO_2 (001): reconstruction, atomic steps, and domains.* Phys. Rev. B **63**, 235402 (2001).

[55] H. Yunbin, O. Dulub, C. Hongzhi, A. Selloni, and U. Diebold. *Evidence for the predominance of subsurface defects on reduced anatase TiO_2(101).* Physical Review Letters **102**, 106105 (2009).

[56] Y. He, A. Tilocca, O. Dulub, A. Selloni, and U. Diebold. *Local ordering and electronic signatures of submonolayer water on anatase TiO_2(101).* Nature Materials **8**, 585 (2009).

[57] F. Seyedeyn-Azad and D.-K. Zhang. *Selective Catalytic Reduction of Nitric Oxide over Cu and Co Ion-exchanged ZSM-5 Zeolite: The Effect of SiO_2/Al_2O_3 Ratio and Cation Loading.* Catalysis Today **68**, 161 (2001).

[58] F. Lonyi, H. E. Solt, Z. Paszti, and J. Valyon. *Mechanism of NO-SCR by methane over Co,H-ZSM-5 and Co,H-mordenite catalysts.* Applied Catalysis B: Environmental **150-151**, 218 (2014).

[59] Y. Li and J. N. Armor. *Selective Catalytic Reduction of NO_x with Methane over Metal Exchanged Zeolites.* Applied Catalysis B: Environmental **2**, 239 (1993).

[60] E. C. Tyo, C. Yin, M. Di Vece, Q. Qian, G. Kwon, S. Lee, B. Lee, J. E. Debartolo, S. Seifert, R. E. Winans, R. Si, B. Ricks, S. Goergen, M. Rutter, B. Zugic, M. Flytzani-Stephanopoulos, Z. W. Wang, R. E. Palmer, M. Neurock, and S. Vajda. *Oxidative Dehydrogenation of Cyclohexane on Cobalt Oxide (Co_3O_4) Nanoparticles: The Effect of Particle Size on Activity and Selectivity.* ACS Catalysis **2**, 2409 (2012).

[61] B. Solsona, I. Vazquez, T. Garcia, T. E. Davies, and S. H. Taylor. *Complete Oxidation of Short Chain Alkanes Using a Nanocrystalline Cobalt Oxide Catalyst.* Catalysis Letters **116**, 116 (2007).

[62] S. Zhang, J.-J. Shan, Y. Zhu, A. I. Frenkel, A. Patlolla, W. Huang, S. J. Yoon, L. Wang, H. Yoshida, S. Takeda, and F. Tao. *WGS Catalysis and In Situ Studies of CoO_{1-x}, $PtCo_n/Co_3O_4$, and Pt_mCo_m/CoO_{1-x} Nanorod Catalysts.* Journal of the American Chemical Society **135**, 8283 (2013).

[63] G. J. La O, A. Sung-Jin, E. Crumlin, Y. Orikasa, M. D. Biegalski, H. M. Christen, and S.-H. Yang. *Catalytic Activity Enhancement for Oxygen Reduction on Epitaxial Perovskite Thin Films for Solid-Oxide Fuel Cells.* Angewandte Chemie International Edition **49**, 5344 (2010).

[64] M. W. Kanan, J. Yano, Y. Surendranath, M. Dinca, V. K. Yachandra, and D. G. Nocera. *Structure and Valency of a Cobalt-phosphate Water Oxidation Catalyst Determined by In Situ X-ray Spectroscopy.* Journal of the American Chemical Society **132**, 13692 (2010).

[65] F. Jiao and H. Frei. *Nanostructured Cobalt Oxide Clusters in Mesoporous Silica as Efficient Oxygen-Evolving Catalysts.* Angewandte Chemie International Edition **48**, 1841 (2009).

[66] B. Solsona, I. Vazquez, T. Garcia, T. E. Davies, and S. H. Taylor. *Complete Oxidation of Short Chain Alkanes Using a Nanocrystalline Cobalt Oxide Catalyst.* Catalysis Letters **116**, 116 (2007).

[67] B. Solsona, T. E. Davies, T. Garcia, I. Vazquez, A. Dejoz, and S. H. Taylor. *Total Oxidation of Propane Using Nanocrystalline Cobalt Oxide and Supported Cobalt Oxide Catalysts.* Applied Catalysis B: Environmental **84**, 176 (2008).

[68] L. P. R. Profeti, E. A. Ticianelli, and E. M. Assaf. *Ethanol Steam Reforming for Production of Hydrogen on Magnesium Aluminate-supported Cobalt Catalysts Promoted by Noble Metals.* Applied Catalysis A: General **360**, 17 (2009).

[69] T.-C. Xiao, S.-F. Ji, H.-T. Wang, K. S. Coleman, and M. L. H. Green. *Methane Combustion Over Supported Cobalt Catalysts.* Journal of Molecular Catalysis A: Chemical **175**, 111 (2001).

[70] M. Li and E. I. Altman. *Shape, Morphology, and Phase Transitions during Co Oxide Growth on Au(111).* The Journal of Physical Chemistry C **118**, 12706 (2014).

[71] M. A. Langell, M. D. Anderson, G. A. Carson, L. Peng, and S. Smith. *Valence-band Electronic Structure of Co_3O_4 Epitaxy on CoO(100).* Phys. Rev. B **59**, 4791 (1999).

[72] M. Chen, B. Hallstedt, and L. Gauckler. *Thermodynamic assessment of the Co-O system.* Journal of Phase Equilibria **24**, 212 (2003).

[73] S. C. Wang and G. Ehrlich. *Structure, stability, and Surface Diffusion of Clusters: Ir_x on Ir(111).* Surface Science **239**, 301 (1990).

[74] S. C. Wang and G. Ehrlich. *Equilibrium Shapes and Energetics of Iridium Clusters on Ir(111).* Surface Science **391**, 89 (1997).